Diagonal static spin correlation in the low temperature orthorhombic Pccn phase of $La_{1.55}Nd_{0.4}Sr_{0.05}CuO_4$

S. Wakimoto*† and J. M. Tranquada Physics Department, Brookhaven National Laboratory, Upton, New York 11973

T. Ono, K. M. Kojima and S. Uchida.

Department of Applied Physics, University of Tokyo, Hongo 7-3-1, Bunkyo, Tokyo 113-8656, JAPAN

S.-H. Lee and P. M. Gehring

National Institute of Standards and Technology, NCNR, Gaithersburg, Maryland 20889

R. J. Birgeneau

Department of Physics and Center for Materials Science and Engineering, Massachusetts Institute of Technology, Cambridge, Massachusetts 02139

and

Department of Physics, University of Toronto, Toronto, Ontario, Canada M5S 1A7 (October 23, 2019)

Elastic neutron scattering measurements have been performed on Nd, Sr co-doped La_{1.55}Nd_{0.4}Sr_{0.05}CuO₄, which exhibits a structural phase transition at $T_s \sim 60$ K from the low temperature orthorhombic Bmab phase (labelled LTO1) to the low temperature orthorhombic Pccn phase (labelled LTO2). At low temperatures, well below T_s , elastic magnetic peaks are observed at the "diagonal" incommensurate (IC) positions $(0,1\pm0.055,0)$, with modulation direction only along the orthorhombic b-axis just as in Nd-free La_{1.95}Sr_{0.05}CuO₄. In the present study, the one-dimensionality of the IC modulation, which is naturally explained by a stripe model, is clearly demonstrated with our "single-domain" crystal. The temperature dependence of the IC peak intensity suggests a substantial contribution from the Nd³⁺ spins below ~ 3 K. Consistent with this, the L dependence of the magnetic scattering is accurately accounted for by a model in which the contribution of the Nd³⁺ spins is explicitly included.

PACS numbers: 74.72.Dn, 75.30.Fv, 75.50.Ee

I. INTRODUCTION

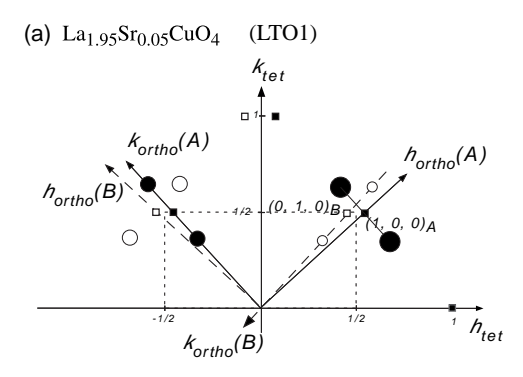
The relationship between the microscopic magnetism and superconductivity is one of the central issues in the field of high- T_C superconductivity. In particular, $La_{2-x}(Sr,Ba)_xCuO_4$ (LSCO, LBCO) and related compounds have received intensive attention because of their rich magnetic and transport properties. In addition, these materials have a simple layered structure with single CuO₂ planes composed of square Cu²⁺ lattices¹; this facilitates the application of theoretical models. It is well known that superconducting LSCO samples exhibit dynamic incommensurate (IC) magnetic correlations modulated along the direction parallel to the Cu-O-Cu bonds in the low-temperature orthorhombic (LTO1, Bmab) structure.²⁻⁴ After the discovery of this IC nature, a systematic neutron-scattering study on the superconducting LSCO compounds⁵ revealed a linear relation between the hole concentration x and the incommensurability parameter δ (Ref. 6) in the under-doped region $(0.06 \le x \le 0.12)$, suggesting a strong correlation between the superconductivity and the dynamic IC

On the other hand, several investigations have been performed at the specific hole concentration $x\sim 1/8$

where for many co-dopants the superconductivity is dramatically suppressed. This so-called 1/8 anomaly was originally discovered in the LBCO system⁷ and found to be associated with a structural transition to the lowtemperature tetragonal (LTT, $P4_2/ncm$) phase.⁸ A similar, but much smaller, suppression of T_C , as well as an enhancement of static magnetic correlations, has been reported in the LSCO system, in which there is no transition to the LTT phase. 9-12 An important clue relevant to the 1/8 anomaly was the observation in the Nd, Sr co-doped $La_{1.48}Nd_{0.4}Sr_{0.12}CuO_4$ compound of very clear elastic magnetic peaks at the parallel IC positions around (π,π) by neutron-scattering. ^{13,14} (The doped Nd³⁺ ions induce the LTT structure as well as the 1/8 anomaly. 15) On the basis of the stripe model¹⁶ it was suggested that charge stripes along the Cu-O-Cu bond, which result in parallel IC peaks, might be pinned by the corrugation of the CuO₂ plane caused by the coherent tilt of the CuO₆ octahedra which is perpendicular to the stripes in the LTT structure. Thence, the elastic IC correlations are enhanced and the superconductivity is more suppressed than in the LTO1 structure of LSCO.

Recently Wakimoto $et~al.^{17,18}$ discovered the so-called "diagonal" IC peaks in insulating $\rm La_{1.95}Sr_{0.05}CuO_4$, which shows the LTO1 structure. The IC peak positions

are shown in Fig. 1(a). In this case, the IC modulation is parallel to the orthorhombic b-axis, which is the same as the coherent tilting direction of the CuO₆ octahedra, and at 45° to the Cu-O bonds. Assuming that the magnetic peaks are associated with charge stripe order, the charge stripes would run parallel to the orthorhombic a-axis. Thus, similar to the case of La_{2-x-y}Nd_ySr_xCuO₄ (LNSCO), the stripes may be pinned by the corrugation of the CuO₂ planes in the LTO1 phase; one might then speculate that the pinning is responsible for the insulating behavior below \sim 100 K. Subsequent experiments by Matsuda $et~al.^{19}$ and by Fujita $et~al.^{20}$ have shown that this diagonal one-dimensional (1D) spin density wave state in LSCO extends across the entire spin-glass region $0.02 \stackrel{<}{\sim} x \stackrel{<}{\sim} 0.06$.



(b) $La_{1.55}Nd_{0.4}Sr_{0.05}CuO_4$ (LTO2)

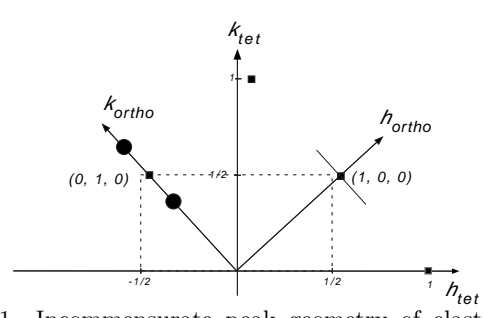


FIG. 1. Incommensurate peak geometry of elastic magnetic peaks observed in La_{1.95}Sr_{0.05}CuO₄ (upper) and La_{1.55}Nd_{0.4}Sr_{0.05}CuO₄ (lower). Circles and squares represent the magnetic and the nuclear Bragg peak positions, respectively. Note that the Bragg peak positions are observed by $\lambda/2$ neutrons. In the upper figure, closed and open symbols correspond to different twin domains.

These facts naturally suggest the importance of research on the relation among the three factors: crystal structure, IC magnetic correlations and the superconductivity. Therefore, it is important to investigate how the magnetic and transport properties change when the corrugation of the CuO_2 plane is changed in $\text{La}_{1.95}\text{Sr}_{0.05}\text{CuO}_4$. With the above as motivation, we performed neutron-scattering experiments and resistivity measurements on $\text{La}_{1.55}\text{Nd}_{0.4}\text{Sr}_{0.05}\text{CuO}_4$ whose corrugation pattern of the CuO_2 planes should be differ-

ent from that of Nd-free La_{1.95}Sr_{0.05}CuO₄. Specifically, La_{1.55}Nd_{0.4}Sr_{0.05}CuO₄ shows the low-temperature orthorhombic (LTO2, Pccn) structure in which the CuO₆ octahedral tilt direction is slightly rotated from the orthorhombic b axis.

The format of this paper is as follows. The sample preparation, details of the experimental procedure and the basic characterizations are described in Sec.II. The results of elastic neutron-scattering experiments are described in Sec.III. We discuss the relation between the structure and magnetic IC modulation in Sec.IV.

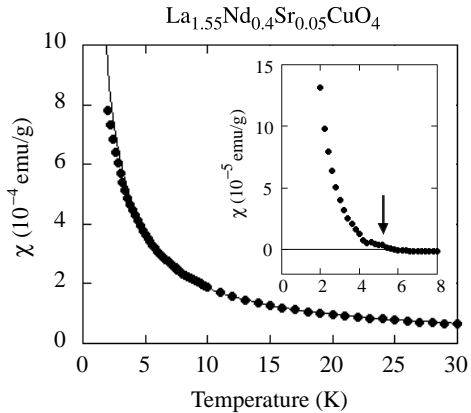


FIG. 2. Temperature dependence of magnetic susceptibility measured under the applied field 0.02 Tesla to an arbitrary direction after the cooling process in zero field. The solid line is fitting result by Curie Law ($\chi = \chi_0 + C/T$) using the data between 5K and 50K. The inset is a differential plot between the measured value and the fitted curve. The arrow indicates the spin-glass transition temperature.

II. SAMPLE PREPARATION AND EXPERIMENTAL DETAILS

Single crystals of $\rm La_{1.55}Nd_{0.4}Sr_{0.05}CuO_4$ were grown by the travelling-solvent floating-zone method at MIT and the University of Tokyo in essentially the same manner, as described below. In the present paper, we label the crystals grown at MIT and the University of Tokyo as samples A and B, respectively.

Dried powders of La₂O₃, Nd₂O₃, SrCO₃ and CuO of 99.99 % purity were mixed and baked in air at 950°C and 1000°C for 24 hours with grinding between each baking. The powder sample so-obtained was confirmed to be a single 2-1-4 phase by X-ray powder diffraction. Feed rods were shaped in rubber tubing pressed by a hydrostatic press, and baked in air at 1100°C for 12 hours. Solvents with the composition of La_{1.55}Nd_{0.4}Sr_{0.05}CuO₄: CuO = 30: 70 in molar ratio were chosen based on the phase diagram for the pure La₂CuO₄ compound.²¹ The growth was performed in a four-ellipsoidal-mirror type image furnace in an oxygen atmosphere. The pelletized

solvent was placed between the feed rod (attached to the upper shaft) and a seed crystal (on the lower shaft), and was melted at the focal point. A crystal was grown by moving the ellipsoidal-mirrors upward. During the high temperature operation of growth, there is vaporization of a small amount of CuO from the molten zone which causes a change in the solvent composition. To avoid this, extra CuO of ~ 1 mol% was added into the feed rods to compensate for the loss of CuO vaporizing from the molten zone during the growth. Since the concentration of Nd and Sr in the crystallized part in the beginning of the growth is possibly different from the nominal one, we continued the growth for more than 100 hours with a growth speed of 0.8 mm/hour to achieve the equilibrium condition; this technique produces a crystal with the nominal composition.

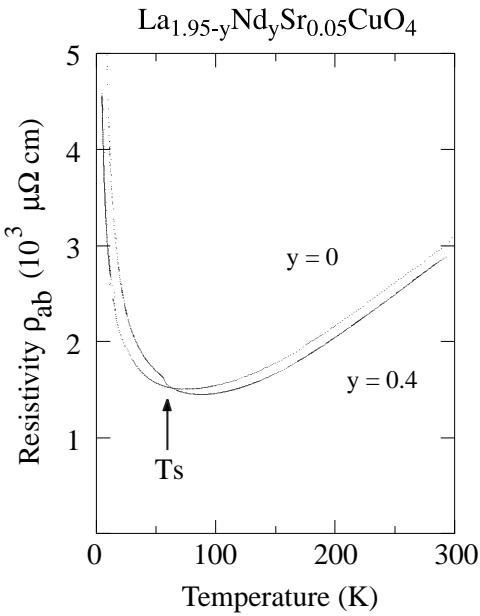


FIG. 3. Temperature dependence of in-plane resistivity for crystal B together with that for the Nd-free sample. The temperature indicated as T_s is the LTO1-LTO2 structural transition temperature.

Since we realized that Nd-free LSCO crystals in the lightly doped region, $0.03 \le x \le 0.05$, tend to absorb excess oxygen in the melt-grown process in an oxygen atmosphere,²² the as-grown crystal was annealed in an Ar atmosphere at 850 °C for 12 hours to purge any excess oxygen. Figure 2 shows the magnetic susceptibility of sample A measured after the treatment in the Ar atmosphere. The measurement was performed by a SQUID magnetometer after the zero field cooling process. The solid line is the result of a fit to Curie law $\chi = \chi_0 + C/T$, where C is the Curie constant, using the data between 5 K and 50 K. There is a small deviation from the Curie law below ~ 5 K due to a spin-glass transition. This is more clearly shown in the inset by plotting the difference between the fitted curve and the data. We also confirmed that sample B shows the same feature. The spin-glass transition at ~ 5 K is consistent with that observed in Nd-free La_{1.95}Sr_{0.05}CuO₄. 22

We also performed resistivity measurements. The measurements were carried out by the standard dc four-probe method using small pieces cut from crystals A and B. Electrodes were attached on the crystal surface with goldpaste. To achieve good contact between the crystal and the electrodes, the crystal with pasted electrodes was annealed at 900 °C in oxygen for an hour. Such short time annealing should not affect the oxygen content significantly. Both crystals A and B show the same resistivity features qualitatively as well as quantitatively. Figure 3 shows the temperature dependence of the resistivity of crystal B together with that of Nd-free La_{1.95}Sr_{0.05}CuO₄. The resistivity shows insulating behavior at low temperature, and there is no superconducting transition. There is a small anomaly at the structural transition temperature, T_s , from the LTO1 to the LTO2 phase at ~ 60 K, consistent with that found for crystal A by neutron-scattering (see Sec. III-A).

Neutron scattering experiments were performed mainly on sample A at the triple-axis spectrometer SPINS installed at the cold neutron guide at the NIST research reactor. The horizontal collimator sequence 32'-40'-S-40'-open and an incident neutron energy E_i =5 meV Pyrolytic graphite (002) was used as were utilized. both monochromator and analyzer. Contamination from higher-order neutrons was eliminated partially with a single Be filter, and completely with two Be filters. We confirmed that there is no significant multiple scattering around (π,π) with this incident energy in elastic scattering measurements. A crystal 40 mm in length for the neutron-scattering experiments was cut from the end part of the grown crystal. The sample was mounted in either the (HK0) or (0KL) scattering plane in a pumped-helium cryostat. The lattice parameters were a = 5.349 Å, b = 5.355 Å and c = 13.012 Å at 1.5 K.

Figure 1(b) shows the scattering geometry in the (HK0) scattering plane of the present LNSCO crystal A. The squares indicate the apparent nuclear Bragg peak positions determined by neutrons with a half wave length $(\lambda/2)$, while the circles indicate the IC elastic magnetic peak positions. Properly, there is no nuclear or magnetic peak at the orthorhombic (100) or (010) positions. The $\lambda/2$ measurement is used to determine precisely the orientation of the IC peaks with respect to the reciprocal lattice (and possible twin domains).

The orthorhombic structure typically has two or more twin domains, as shown in Fig. 1(a), which indicates the nuclear and magnetic peak geometry in the Nd-free x=0.05 crystal containing two twin-domains. However, in the present crystal A, one of the domains is so dominant that one can treat it as effectively a single domain crystal. Indeed, only a single pair of the diagonal type IC peaks is clearly observed around the (010) position (see Sec. III and IV). Detailed neutron-scattering experiments have been performed mainly on crystal A because crystal B is smaller and has at least two twin

domains with almost the same population. However, it should be noted that we confirmed the same 1D nature of the IC magnetic peaks also in crystal B. In section III, the detailed magnetic cross-section of crystal A is reported.

Since the orthorhombic crystallographic axes in both the LTO1 and LTO2 structures are defined by the diagonals of the distorted squares of the ${\rm CuO_2}$ lattice, the orthorhombic a^* and b^* axes in reciprocal space are defined as shown in Fig. 1. Throughout the present paper, indices based on the orthorhombic Bmab or Pccn crystallographic notation are utilized. Since clear IC magnetic peaks are observed only around (010), we utilized the (0KL) scattering plane to measure the L dependence of the IC peak intensity so that the high-intensity peaks lie in the scattering plane.

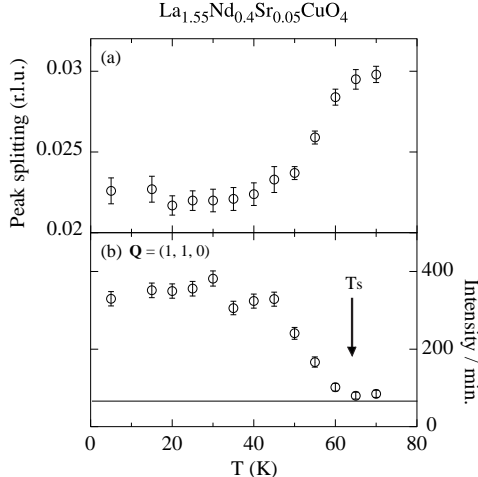


FIG. 4. Temperature dependence of (a) orthorhombic splitting between (200) and (020), and (b) intensity of superlattice peak for *Pccn* structure at (110).

III. EXPERIMENTAL RESULTS

A. Structural transition to the LTO2 phase

Although one twin domain is dominant in the present crystal, there are some other minor twin domains whose volume is estimated to be less than 1/4 of that of the dominant domain. Therefore, we were able to observe the orthorhombic splitting between the (200) peak of the dominant domain and the (020) peak in a minor domain. Figure 4(a) shows the temperature dependence of the splitting. On cooling, the orthorhombicity decreases by about 30 % between 65 K and 40 K. The intensity of the (110) peak, which is a superlattice peak of the *Pccn* structure but not of the Bmab structure, appears and increases in a complementary manner as shown in Fig. 4(b). These facts demonstrate that the system indeed exhibits a structural transition from the Bmab LTO1 phase to the *Pccn* LTO2 phase. The transition temperature of ~ 65 K agrees well with that expected from the phase diagram previously reported by Crawford $et\ al.^{15}$ This transition temperature is also in reasonable agreement with that of crystal B determined from the resistivity measurement.

In the LTO1 structure above 65 K, the CuO₆ octahedra tilt along the orthorhombic b-axis. In the LTO2 structure, the octahedra tilt along a direction rotated within the plane away from the b-axis. From the change of the orthorhombic splitting in Fig. 4, the shift of the tilt direction from the b-axis is estimated to be ~ 15 degrees.

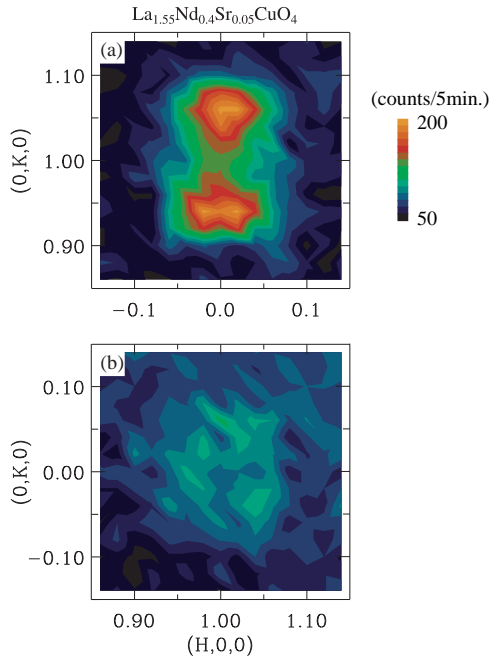


FIG. 5. Contour plots of magnetic peak intensity around (a) (010) and (b) (100). Incommensurate peak positions are summarized in Fig. 1(b) by closed squares.

B. Magnetic cross section

Contour plots of the elastic neutron-scattering intensity around (010) and (100) are shown in Figs. 5(a) and 5(b), respectively. Since the crystal has a single dominant twin domain, the 1D nature of the IC modulation along the orthorhombic b-axis is clearly observable in Fig. 5(a); it is consistent with, but more obvious than, that first reported for the Nd-free x = 0.05 sample. 18 An important difference from the Nd-free x = 0.05 compound is that clear magnetic peaks appear only around the (010) position; for the Nd-free sample, the intensity is strongest for the peaks split about (100). (The two cases are schematically summarized in Fig. 1.) A similar change of the magnetic peak position from (100) to (010) has been previously reported in Sr-free $La_{2-y}Nd_yCuO_4$. This feature is discussed in Sec.IV in terms of the spin orientation.

To analyze the IC peaks in detail, we made scans through the peak positions in the vicinity of (010) with higher statistics, achieved by optimizing the vertical focusing of the incident neutron beam. Figures 6(a) and 6(b) show the peak profiles along the trajectories α and β indicated by arrows in Fig. 6(c). The incommensurate peaks are observed at the $(0,1\pm\epsilon,0)$ positions. (The IC peak intensity in unit time is different from that in Fig. 5 due to the change in the vertical focusing of the incident beam; however, the vertical focusing does not affect the intrinsic characteristic values, such as the width, positions and temperature dependence of the IC peaks.)

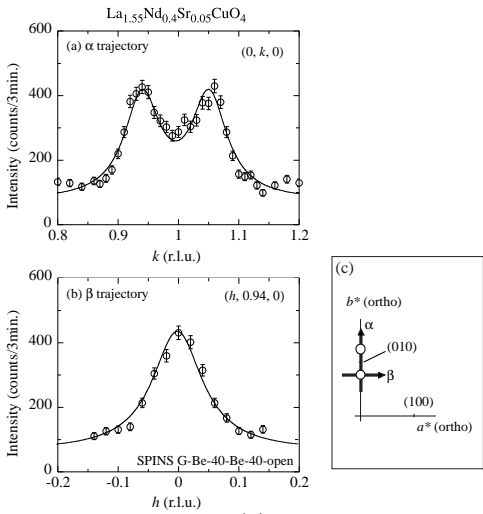


FIG. 6. Peak profiles along (a) the α trajectory and (b) the β trajectory shown in (c). Solid lines are fitting results by Lorentzian function. By this fitting, the incommensurability parameter ϵ is ~ 0.055 .

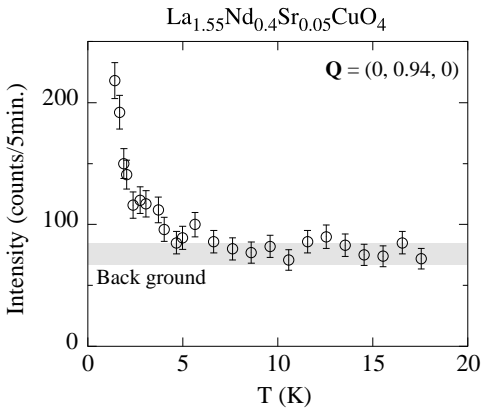


FIG. 7. Temperature dependence of elastic IC magnetic peak at (0, 0.94, 0).

The solid lines in Fig. 6 are fitted curves corresponding to a two-dimensional Lorentzian function convoluted with the instrumental resolution. The intrinsic peak half widths along the a^* and b^* directions are $\kappa_a = 0.053 \, \text{Å}^{-1}$ and $\kappa_b = 0.039 \, \text{Å}^{-1}$, respectively. The incommensurability parameter is $\epsilon = 0.055(\pm 0.004)$, which is slightly lower than that for Nd-free x = 0.05, where $\epsilon = 0.064$. Although in the contour plot of Fig. 5(b) the peak at

 $(0, 1 - \epsilon, 0)$ seems to be split additionally along the a^* -axis, the profile in Fig. 6(b) with higher statistics shows a single peak centered at h = 0.

The temperature dependence of the IC peak at (0, 0.94, 0) is shown in Fig. 7. This measurement was done without optimizing the vertical focusing. The intensity gradually increases with decreasing temperature below $\sim 5~\rm K$ and rapidly increases below $\sim 3~\rm K$. From previous experience with Nd-doped samples, 14 we expect that this additional increase of intensity below $\sim 3~\rm K$ is caused by an additional ordering of the Nd $^{3+}$ spins.

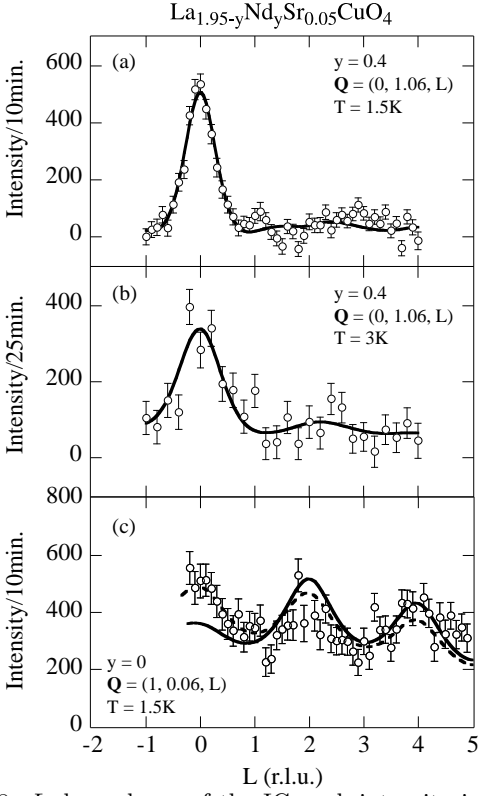


FIG. 8. L dependence of the IC peak intensity in (a) the Nd,Sr co-doped sample at 1.5K, (b) the Nd,Sr co-doped sample at 3K, and (c) the Nd-free sample at 1.5K (obtained from Ref. 18). The back ground intensity at 30K have been subtracted. Solid lines in (a) and (b) are the results of fit by a model including contribution from Nd³⁺ spins and out-of-plane component of Cu^{2+} spins. (See text). Solid line in (c) is the fit with the same model without Nd³⁺ spin contribution and out-of-plane component of Cu^{2+} , while dashed line is the fit without only Nd³⁺ spin component.

The L dependences of the intensity at the IC position (0,0.94,L) at 1.5 K and 3 K are shown in Figs. 8(a) and 8(b), respectively. For both results, the intensity at 30 K was subtracted as background so that the intensities shown are purely magnetic. We fit the data with a model introduced previously in a study of the Nd-doped x=0.12 compound. 14 The model has the form:

$$I(L) \propto |F|^2 \frac{1 - t^2}{1 + t^2 - 2t\cos(\pi L)}.$$
 (1)

This function consists of the magnetic structure factor F and an oscillating function, with line width determined by $t = \exp(-c/\xi)$, where ξ is a correlation length. In the analysis of the Nd-doped x = 0.12 results, an oscillation period of L = 1 was utilized. This was an appropriate choice in that case because of the assumed rotation of the stripe orientation by 90° from one CuO₂ plane to the nearest neighbor plane, which gives rise to correlations between the next nearest neighbor planes. However, in the present system with x = 0.05 the IC modulation is only along the orthorhombic b-axis, that is, a 90° rotation of the stripe orientation is not likely. Thus, we utilized the oscillation function with a period of L = 2.

The structure factor is described as

$$|F|^2 = p_{\text{Cu},\parallel}^2 f_{\text{Cu}}^2 + [p_{\text{Cu},\perp} f_{\text{Cu}} + y p_{\text{Nd}} f_{\text{Nd}} \cos(2\pi L z_{\text{Nd}})]^2.$$
(2)

In this equation, f_{Cu} and f_{Nd} are **Q**-dependent magnetic form factors for the Cu^{2+} and Nd^{3+} spins which are taken from the literature. 25,26 z_{Nd} is the distance between Nd and the nearest Cu in units of c, which has been determined to be 0.36 by a neutron powder diffraction study.²⁷ p is the spin component perpendicular to the scattering vector **Q**, which relates to the ordered magnetic moment μ by $\mathbf{p} = \vec{\mu} - \hat{\mathbf{Q}}(\hat{\mathbf{Q}} \cdot \vec{\mu})$. The indices \parallel and \perp represent in-plane and out-of-plane components of the Cu²⁺ spin, respectively. Since the Nd³⁺ spins are assumed to be parallel to the c-axis, the first term describes the contribution of the in-plane component of the Cu²⁺ spins while the second term describes contributions of out-ofplane components of both the Cu^{2+} and Nd^{3+} spins. We assumed the spin direction of \mathbf{p}_{\parallel} to be random because the system shows the features of a spin-glass. The fitting results are shown by the solid lines in Figs. 8(a) and 8(b), which agree with the experimental results.

In order to check the consistency of this function, we also fit the L dependence of the IC peak intensity for the Nd-free x=0.05 compound reported in Ref. 18 with the function presented above without the Nd³⁺ spin contribution. Since the out-of-plane component of the Cu²⁺ spins $p_{\text{Cu},\perp}$ is assumed to be driven by the interaction with the Nd³⁺ spins in the present model, we fit the data with $p_{\text{Cu},\perp}$ fixed at zero. The fitted curve is shown in Fig. 8(c) by the solid line. For comparison, we also fit

TABLE I. Parameters obtained in fitting to the L dependences by Eq. (1). μ is ordered magnetic moment which relates to p in Eq. (2) by $\mathbf{p} = \vec{\mu} - \mathbf{\hat{Q}}(\mathbf{\hat{Q}} \cdot \vec{\mu})$. The values listed at the bottom are given by the fitting for the y = 0 sample data with $p_{\mathrm{Cu},\perp}$ as a fitting valuable.

| y and $T(K)$ | $\mu_{\mathrm{Cu},\perp}/\mu_{\mathrm{Cu},\parallel}$ | $\mu_{ m Nd}/\mu_{ m Cu}$ | ξ/c |
|------------------|---|---------------------------|-------------------|
| y = 0.4, T = 1.5 | 0.96 ± 0.25 | 4.1 ± 0.9 | 0.58 ± 0.11 |
| y = 0.4, T = 3 | 1.04 ± 0.37 | 1.1 ± 0.6 | 0.36 ± 0.18 |
| y = 0, T = 1.5 | 0 | 0 | 0.48 ± 0.05 |
| | (0.55 ± 0.05) | (0) | (0.44 ± 0.04) |

the data with $p_{\mathrm{Cu},\perp}$ as a fitting variable, as shown by the dashed line.²⁸

The parameters obtained by fitting in Fig. 8 are summarized in Table 1. The values listed in the bottom row are obtained by fitting the Nd-free data with a $p_{\mathrm{Cu},\perp}$ component. In the Nd-doped sample, the out-of-plane component of the Cu^{2+} spins is larger than that in the Nd-free sample even if we assume the Nd-free sample also has an out-of-plane component. This indicates that the the out-of-plane component of the Cu^{2+} spins is induced by the correlation with the Nd $^{3+}$ spins parallel to the c-axis. For the Nd-doped sample, the ratio $\mu_{\mathrm{Nd}}/\mu_{\mathrm{Cu}}$ increases with decreasing temperature, consistent with the rapid increase of the IC intensity below 3 K in Fig. 7.

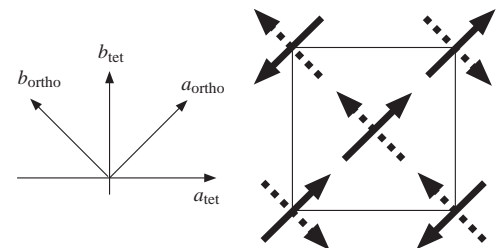


FIG. 9. Schematic figure of the spin structure. The square represents CuO₂ square lattice. The arrows at the corners are spins of the Cu²⁺ ions on the same plane and the arrows at the center are spins on the nearest neighbor plane. The spin structure shown by the dashed and solid arrows give the magnetic bragg peaks at (100) and (010), respectively.

IV. DISCUSSION

The present paper reports the IC magnetic order observed by neutron-scattering experiments for the ${\rm La_{1.55}Nd_{0.4}Sr_{0.05}CuO_4}$ compound. One of the important results is that the same type of 1D IC spin modulation as that reported for the Nd-free x=0.05 compound¹⁸ is clearly observed in the almost single twin-domain sample of Nd-doped x=0.05. This demonstrates that the 1D IC modulation along the orthorhombic b-axis is common in the lightly Sr-doped spin-glass systems with both LTO1 and LTO2 structure.

A major difference from the Nd-free sample is that the clear IC peaks appear around the (010) position in the present LTO2 compound, while a more intense pair of peaks appears around (100) in the Nd-free x=0.05. A similar change of the magnetic peak position from (100) to (010) has been reported by powder neutron-scattering for La_{1.8}Nd_{0.2}CuO₄ (Ref. 23); the magnetic commensurate peak at (100) in the LTO1 phase shifts to (010) below the LTO1-LTO2 transition temperature. Such a change of the magnetic peak position can be explained simply by a rotation of the spin direction that causes a change of the antiferromagnetic propagation vector from the \hat{a} to the \hat{b} direction. This change is schematically drawn in Fig. 9. The square represents the CuO₂ square lattice. The arrows at the corners are spins of the Cu²⁺

ions on the same CuO_2 plane while the arrows at the center are spins on the nearest neighbor plane.

The spin structure shown by the dashed arrows has the propagation vector along \hat{a} and gives a magnetic peak at (100). On the other hand, the structure shown by the solid arrows has the propagation vector along \hat{b} and accordingly gives the peak at (010). The latter spin orientation, with the modulation along the b-axis, is consistent with the strong IC peak intensity around (010) as observed in the present LTO2 compound. The change between the two magnetic structures is realized by the opposite rotation of the spin directions in neighboring planes; that is, the spins on one plane rotate clockwise uniformly while those in the nearest-neighbor plane rotate counter-clockwise. Such an alternative rotation across the LTO1-LTO2 transition temperature has also been identified in a neutron-scattering study of La_{1.65}Nd_{0.35}CuO₄ by comparing the peak intensity at L = 0 and L = 1. (Ref. 24)



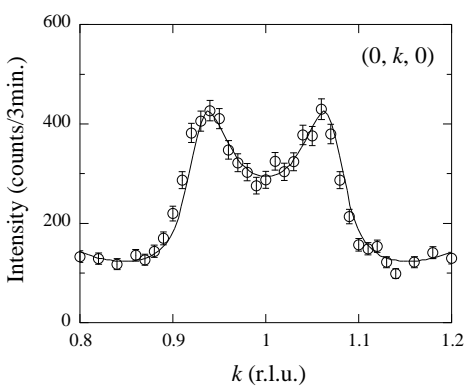


FIG. 10. Upper panel shows expected stripe structure in the present LNSCO sample. White circles and arrows represent Cu atoms and their spins. The shaded regions are charge stipes. The lower panel is the IC peak profile with the fitted curve using the stripe model. (See text.)

Another difference between Nd-doped and Nd-free samples can be seen in the IC peak width. From fitting with the same two-dimensional Lorentzian function convoluted with the instrumental resolution, the intrinsic widths for the present crystal are determined to be $\kappa_a=0.053~\text{Å}^{-1}$ and $\kappa_b=0.039~\text{Å}^{-1}$, which are slightly larger than those for the Nd-free x=0.05 sample, $\kappa_a\sim0.04~\text{Å}^{-1}$ and $\kappa_b\sim0.03~\text{Å}^{-1}$. (Ref. 18) In order to check whether this larger width is intrinsic to the LTO2 structure, a more systematic comparison between the LTO2 and LTO1 phases is required.

Finally, we discuss the stripe model. Among the the-

oretical explanations for the IC feature, the 1D modulation observed in the present study is most easily understood in terms of the stripe model¹⁶. Therefore, we tried to analyze the IC peak profile by the stripe model. Specifically, we fit the profile in Fig. 5(a) by a function which has been introduced based on the stripe model²⁹:

$$I(k) \propto |F'|^2 \frac{1 - q^2}{1 + q^2 - 2q\cos(2\pi nk)}.$$
 (3)

where $q = (-1)^{n+1} \exp(-nb/\xi)$ and n is the stripe spacing in the orthorhombic lattice unit. F' is the magnetic structure factor for a single antiferromagnetic region between nearest charge stripes. This function gives the oscillation modified by the antiferromagnetic structure factor.

In the present system, the charge stripes are parallel to the orthorhombic a-axis and have the spacing nb as schematically shown in the upper panel of Fig. 10. (This figure corresponds to the spacing n=7.) Therefore, the magnetic structure factor F' can be described approximately as a function of k:

$$F' \propto 1 + 2 \sum_{j=1}^{n-1} (-1)^j \cos(\pi j k).$$
 (4)

The actual fitted curve using Eqs. (3) and (4) with fixed n=7 is indicated by the solid line in Fig. 10. The only fitting parameter, ξ , is ~ 31 Å. (The stripe spacing n=7 is smaller than the expected value n=8 from the incommensurability $\epsilon \sim 0.06$ r.l.u. However, in the fitting with n = 8, the damping by the magnetic structure factor is stronger than that for n = 7 and results in poorer agreement with the data.) Figure 10 demonstrates that this model gives a reasonable description of the experimental data. As noted in section III, in the comparison of the incommensurability parameter ϵ determined by the Lorentzian function fit, the Nd-doped sample has the incommensurability, $\epsilon = 0.055$, which is slightly smaller than that for Nd-free sample, $\epsilon = 0.064$. However, in the fitting using the stripe function, the fit with the fixed parameter n = 7 also agrees reasonably with the experimental data for Nd-free x = 0.05 with the fitting variable $\xi \sim 47$ Å. Thus the stripe structure can explain the IC peaks also in the lightly hole doped region with a stripe spacing of 7b for x = 0.05 compounds.

As a future experiment, it would be interesting to see whether an in-plane anisotropy of the conductivity, associated with the 1D magnetic modulation, can be observed in an untwinned crystal with $x \leq 0.05$, where the unique orientation of the IC modulation has been observed.

V. ACKNOWLEDGEMENT

We thank Y. Endoh, K. Hirota, and G. Shirane for invaluable discussions. The work at Brookhaven National Laboratory was carried out under Contract No.

DE-AC02-98CH10886, Division of Materials Sciences, U. S. Department of Energy. The work at MIT was supported by the NSF under Grant No. DMR0071256 and by the MRSEC Program of the National Science Foundation under Award No. DMR98-08941. The work at the University of Tokyo was financially supported by Grantin-Aid for Scientific Research from the Ministry of Education, Science, Sports and Culture of Japan. The work at SPINS in National Institute of Standards and Technology is based upon activities supported by the National Science Foundation under Agreement No. DMR-9986442.

- ★ Also at Department of Physics, Massachusetts Institute of Technology, Cambridge, MA 02139.
- † Present address: Department of Physics, University of Toronto, Toronto, Ontario, Canada M5S 1A7.
- ¹ M. A. Kastner, R. J. Birgeneau, G. Shirane, and Y. Endoh, Rev. Mod. Phys., **70**, 897 (1998).
- ² H. Yoshizawa, S. Mitsuda, H. Kitazawa, and K. Katsumata, J. Phys. Soc. Jpn. 57, 3686 (1988).
- ³ R. J. Birgeneau, Y. Endoh, Y. Hidaka, K. Kakurai, M. A. Kastner, T. Murakami, G. Shirane, T. R. Thurston, and K. Yamada, Phys. Rev. B **39**, 2868 (1989); T. R. Thurston, R. J. Birgeneau, M. A. Kastner, N. W. Preyer, G. Shirane, Y. Fujii, K. Yamada, Y. Endoh, K. Kakurai, M. Matsuda, Y. Hidaka, and T. Murakami, *ibid* **40**, 4585 (1989).
- ⁴ S. -W. Cheong, G. Aeppli, T. E. Mason, H. A. Mook, S. M. Hayden, P. C. Canfield, Z. Fisk, K. N. Klausen, and J. L. Martinez, Phys. Rev. Lett. 67, 1791 (1991).
- ⁵ K. Yamada, C. H. Lee, K. Kurahashi, J. Wada, S. Wakimoto, S. Ueki, H. Kimura, Y. Endoh, S. Hosoya, G. Shirane, R. J. Birgeneau, M. Greven, M. A. Kastner, and Y. J. Kim, Phys. Rev. B **57**, 6165 (1998).
- ⁶ Incommensurability parameter δ is defined by splitting width of IC peaks in the reciprocal space. Specifically, the IC peak positions are described with δ as $(1/2\pm\delta,1/2)$ and $(1/2,1/2\pm\delta)$ in the tetragonal I_4/mmm notation.
- ⁷ A. R. Moodenbaugh, Youwen Xu, M. Suenaga, T. J. Folkerts, and R. N. Shelton, Phys. Rev. B 38, 4596 (1988).
- ⁸ J. D. Axe, A. H. Moudden, D. Hohlwein, D. E. Cox, K. M. Mohanty, A. R. Moodenbaugh, Phys. Rev. Lett. **62**, 2751 (1989).
- ⁹ K. Kumagai, K. Kawano, I. Watanabe, K. Nishiyama, and K. Nagamine, J. Supercond. 7, 63 (1994).
- ¹⁰ T. Goto, S. Kazama, K. Miyagawa, and T. Fukase, J. Phys. Soc. Jpn. **63**, 3494 (1994).
- ¹¹ T. Suzuki, T. Goto, K. Chiba, T. Shinoda, T. Fukase, H. Kimura, K. Yamada, M. Ohashi, and Y. Yamaguchi, Phys. Rev. B 57, 3229 (1998).
- ¹² H. Kimura, K. Hirota, H. Matsushita, K. Yamada, Y. Endoh, S.-H. Lee, C. F. Majkrzak, R. Erwin, G. Shirane, M. Greven, Y. S. Lee, M. A. Kastner, and R. J. Birgeneau, Phys. Rev. B 59, 6517 (1999) and private communication.

- ¹³ J. M. Tranquada, B. J. Sternlieb, J. D. Axe, Y. Nakamura, and S. Uchida, Nature **375**, 561 (1995).
- ¹⁴ J. M. Tranquada, J. D. Axe, N. Ichikawa, Y. Nakamura, S. Uchida, and B. Nachumi, Phys. Rev. B 54, 7489 (1996).
- ¹⁵ M. K. Crawford, R. L. Harlow, E. M. McCarron, W. E. Farneth, J. D. Axe, H. Chou, and Q. Huang, Phys. Rev. B 44, 7749 (1991).
- V.J. Emery and S.A. Kivelson, Physica C 235-240, 189 (1994); V.J. Emery, S.A. Kivelson, and O. Zachar, Phys. Rev. B 56, 6120 (1997); C. Nayak and F. Wilezek, Phys. Rev. Lett. 78, 2465 (1997); S.A. Kivelson, E. Fradkin, and V.J. Emery, Nature (London) 393 550 (1998);.
- ¹⁷ S. Wakimoto, G. Shirane, Y. Endoh, K. Hirota, S. Ueki, K. Yamada, R. J. Birgeneau, M. A. Kastner, Y. S. Lee, P. M. Gehring, and S. H. Lee, Phys. Rev. B 60, R769 (1999).
- ¹⁸ S. Wakimoto, R. J. Birgeneau, M. A. Kastner, Y. S. Lee, R. Erwin, P. M. Gehring, S. H. Lee, M. Fujita, K. Yamada, Y. Endoh, K. Hirota, and G. Shirane, Phys. Rev. B **61**, 3699 (2000).
- ¹⁹ M. Matsuda, M. Fujita, K. Yamada, R. J. Birgeneau, M. A. Kastner, H. Hiraka, Y. Endoh, S. Wakimoto, and G. Shirane, Phys. Rev. B. **62**, 9148 (2000).
- ²⁰ M. Fujita, K. Yamada, H. Hiraka, S. H. Lee, P. M. Gehring, S. Wakimoto, and G. Shirane, cond-mat/0101320.
- ²¹ H. Kojima and I. Tanaka, Jpn. J. Appl. Phys. **7**, 76 (1992).
- ²² S. Wakimoto, S. Ueki, Y. Endoh, and K. Yamada, Phys. Rev. B **62**, 3547 (2000).
- ²³ M. K. Crawford, R. L. Harlow, E. M. MacCarron, W. E. Farneth, N. Herron, H. Chou, and D. E. Cox, Phys. Rev. B 47, 11623 (1993).
- ²⁴ B. Keimer, R. J. Birgeneau, A. Cassanho, Y. Endoh, M. Greven, M. A. Kastner, and G. Shirane, Z. Physik B 91, 373 (1993).
- ²⁵ S. Shamoto, M. Sato, J. M. Tranquada, B. J. Sternlieb, and G. Shirane, Phys. Rev. B 48, 13817 (1993).
- ²⁶ M. Blume, A. J. Freeman, and R. E. Watson, J. Chem. Phys. **37**, 1245 (1962).
- ²⁷ J. D. Axe and M. K. Crawford, J. Low Temp. Phys. **95**, 271 (1994).
- ²⁸ Although, from the basic assumption in the model of Eq. (2), the Nd-free sample is supposed to have no $p_{\text{Cu},\perp}$ component, the fitting with the finite value of $p_{\text{Cu},\perp}$ shown by the dashed line in Fig. 8(c) seems to show better agreement with the experimental data. However, we should note that the contamination at L=-0.5 as noted in Ref. 18 may cause a discrepancy between the data and the solid line fitted with $p_{\text{Cu},\perp}=0$.
- ²⁹ J. M. Tranquada, cond-mat/9702117.